This article has been accepted for publication in a future issue of this journal, but has not been fully edited. Content may change prior to final publication. Citation information: DOI 10.1109/TNSRE.2015.2410176, IEEE Transactions on Neural Systems and Rehabilitation Engineering

Real-time Task Discrimination for Myoelectric Control Employing Task-Specific Muscle Synergies

Ghulam Rasool, Kamran Iqbal, *Senoir Member, IEEE*, Nidhal Bouaynaya, *Member, IEEE* and Gannon White

***Abstract*—We present a novel formulation that employs task-specific muscle synergies and state-space representation of neural signals to tackle the challenging myoelectric control problem for lower arm prostheses. The proposed framework incorporates information about muscle configurations, e.g., muscles acting synergistically or in agonist/antagonist pairs, using the hypothesis of muscle synergies. The synergy activation coefficients are modeled as the latent system state and are estimated using a constrained Kalman filter. These task-dependent synergy activation coefficients are estimated in real-time from the electromyogram (EMG) data and are used to discriminate between various tasks. The task discrimination is helped by a post-processing algorithm that uses posterior probabilities. The proposed algorithm is robust as well as computationally efficient, yielding a decision with $> 90\%$ discrimination accuracy in approximately 3 ms. The real-time performance and controllability of the algorithm were evaluated using the targeted achievement control (TAC) test. The proposed algorithm outperformed common machine learning algorithms for single- as well as multi-degree-of-freedom (DOF) tasks in both off-line discrimination accuracy and real-time controllability ($p < .01$).**

***Index Terms*—Myoelectric control, EMG, Muscle synergies, constrained Kalman filter, single- and multi-DOF tasks.**

I. Introduction

The pattern classification algorithms that may identify repeatable patterns of muscle activations have been successfully employed for task discrimination in the myoelectric control [1]. In the pattern classification framework, an analysis window of the electromyogram (EMG) data is formed and a set of representative features is extracted. Classification algorithms are trained using extracted features to discriminate between various tasks. Pattern classification systems have produced promising results in terms of classification accuracy (generally $>$90%) and real-time performance [1], [2]. Though conventional pattern classification algorithms have helped extract movement intent from the myoelectric signals [3], [4], their clinical viability is not commensurate with their classification accuracy [5], [6]. In essence, a true multifunction and dexterous bionic limb with a natural movement control algorithm has yet to be realized [6]. One reason for this shortcoming may have been that the pattern classification systems do not take into account available information about the underlying system physiology. In particular, crucial information involving the underlying neural processes generating the observable muscle activation patterns cannot be explicitly incorporated into pattern classification systems. For example, while performing a reaching or grasping task, some muscles in the forearm may act synergistically or in agonist/antagonist pairs, depending on their physiological configuration and task requirements. Such physiologically relevant information cannot be explicitly incorporated into generic machine learning algorithms, e.g., the linear discriminant analysis (LDA), a commonly used algorithm in myoelectric control applications [3], [7]. In this paper, we develop an alternative approach to task discrimination that readily incorporates muscle synergy information into the modeling and problem solving framework.

Muscle synergies are hypothesized as discrete elements or primitive building blocks for generation of purposeful behavior by the central nervous system (CNS) [8]. By definition, muscle synergies are *fixed relative activation levels of different muscles* [8]. It is hypothesized that the CNS may employ muscle synergies to recruit a large number of muscles using a smaller number of independent control signals (the synergy activation coefficients) [8]. Furthermore, shared and task-specific muscle synergies may also exist [9] and an optimal motor behavior might result from a combination of shared and task-specific muscle synergies [10]. Mathematically, muscle synergies can be interpreted as the basis functions for efficient representation of muscle activations in a lower-dimensional subspace [11]. The hypothesis of muscle synergies assumes that the synergy matrix linearly transforms the activation coefficients descending from the CNS into individual muscular activations. Whether the CNS employs such a low-dimensional embedding for generating purposeful behavior or not is still an open question and authors have generally avoided associating physiological relevance to synergies [12]. This study shows that the hypothesis of muscle synergies carries relevance for real-time task discrimination and subsequent control of a virtual myoelectric prosthetic limb.

Recently, the hypothesis of muscle synergies has been successfully employed in multiple research studies to control prosthetic devices in real-time [13]–[16]. For example, Choi and Kim employed a non-negative muscle synergy matrix to map muscle activities in the forearm into four predefined wrist movement intents (flexion/extension and radial/ulnar deviation) [14]. Similarly, Jiang et al. employed muscle synergies for simultaneous and proportional control of two degrees-of-freedom (DOFs) with promising results [16]. The authors em-

G. Rasool is with the Sensory Motor Performance Program of the Rehabilitation Institute of Chicago, Chicago, IL 60611 USA (email: ghulamrasool@northwestern.edu).

K. Iqbal is a Professor with the Systems Engineering Department, University of Arkansas at Little Rock, Little Rock, AR-72204, USA (email: kxiqbal@ualr.edu).

N. Bouaynaya is an Assistant Professor with the Department of Electrical and Computer Engineering, Rowan University, Glassboro, NJ-08028, USA (email: bouaynaya@rowan.edu).

G. White is an Assistant Professor with the Department of Health, Human Performance, and Sports Management, University of Arkansas at Little Rock, Little Rock, AR-72204, USA (email: gawhite@ualr.edu).

This article has been accepted for publication in a future issue of this journal, but has not been fully edited. Content may change prior to final publication. Citation information: DOI 10.1109/TNSRE.2015.2410176, IEEE Transactions on Neural Systems and Rehabilitation Engineering

ployed the nonnegative matrix factorization (NMF) algorithm to extract muscle synergies, which were later used to obtain the control signals in real-time for simultaneous control of wrist flexion/extension and pronation/supination. In this study, we adopt a similar synergies based approach to the task discrimination problem. We primarily focus on involving three basic DOFs that included pronation/supination, flexion/extension and hand open/close, and their simultaneous combinations, i.e., 6 single-DOF tasks and 12 two-DOF tasks (treating them as separate tasks, in contrast to the simultaneous approach as in [16]). Furthermore, Matrone et al. have previously employed the principal component analysis (PCA) technique to drive two-DOF multi-fingered hand prosthesis in real-time [15]. In this study, we employ probabilistic independent component analysis (pICA) to obtain task-specific muscle synergies. We additionally develop a state-space process dynamics model and use a constrained Kalman filter to estimate the control signals in real-time. The proposed **M**uscle **S**ynergy based task **D**iscrimination (MSD) algorithm outperforms conventional discrimination schemes (referred to as academic state-of-the-art in [16]) in off-line classification accuracy as well as real-time controllability evaluated using the targeted achievement control (TAC) test [17].

The paper is organized as follows: in section II, we outline our mathematical model using the state-space representation of neural signal evolution and the hypothesis of muscle synergies. We also discuss estimation of the activation coefficients, task discrimination, and post-processing in the same section. In Section III, we provide experimental details for EMG data collection and data processing. We present our results and discussion in Sections IV and V, respectively.

II. Mathematical Model and Analytic Methods

To address the task discrimination problem for lower arm prosthesis, we seek a mathematical model that would allow us to use EMG data to discriminate between a set of tasks in real-time. The hypothesis of muscle synergies allows us to capture the temporal evolution of the task-dependent neural control signals, or the synergy activation coefficients that are hypothesized to originate from the CNS and terminates at the peripheral muscles. These activation coefficients represent the contribution of each muscle synergy towards the final muscular activation during performance of a task. The proposed mathematical model allows us to estimate the activation coefficients using real-time EMG data and the task-specific muscle synergy matrices. The task-specificity of these synergies allows us to discriminate between different tasks.

A. The State-Space Model

The state-space representation consists of a process dynamics model that captures the temporal evolution of the system state, and a measurement model, which represents the relationship between the system state and the system output [18]. We adopt a white noise driven state-space model [19] to capture the evolution of the EMG signals. In such representation, the activation coefficients act as the state of the system, whereas the EMG data, i.e., the muscular activations, represent the system output. The state-space representation includes a random walk model for the process dynamics complemented by muscle synergies in the measurement model, and is given as:

$$\mathbf{x}_{k+1} = \mathbf{x}_k + \mathbf{w}_k, \tag{1a}$$

$$\mathbf{y}_k = W\mathbf{x}_k + \mathbf{v}_k, \tag{1b}$$

where $\mathbf{x}_k \in \mathbb{R}^{n_x}$ represents the system state, i.e., the activation coefficients, $\mathbf{y}_k \in \mathbb{R}^{n_y}$ represents the system output (the EMG signal), $W \in R^{n_y} \times R^{n_x}$ is the synergy matrix, $k \in \mathbb{N}$ is the time index, n_x and n_y are the dimensions of the system state (number of muscle synergies) and the output (number of channels of the EMG signal) respectively. $\mathbf{w}_k$ and $\mathbf{v}_k$ are zero-mean process and measurement noise sequences respectively with known Gaussian probability density functions, i.e., $\mathbf{w}_k \in \mathcal{N}(\mathbf{0}, Q_k)$ and $\mathbf{v}_k \in \mathcal{N}(\mathbf{0}, R_k)$. It is known that the surface EMG recorded from bipolar electrodes during constant force constant-angle non-fatiguing contractions can be well modeled as a zero-mean, correlation-ergodic, random process which is Gaussian distributed [20], [21]. However, the Gaussian assumption may not hold during dynamic contractions [20], [21]. Nonetheless, the Kalman filter is the optimal estimator when the noise is Gaussian; and is also the best linear estimator for non-Gaussian noise [22].

A random walk model was chosen to represent process dynamics in order to ensure a smooth time-evolution of the state. The model also reflects lack of *a priori* knowledge about the process dynamics. The measurement model (1b), derived from the hypothesis of muscle synergies, relates the recorded EMG signal $\mathbf{y}_k$ to the latent system state $\mathbf{x}_k$ through a linear mapping, i.e., the muscle synergy matrix W. The mathematical model (1) can be expressed in terms of probability density functions [23] to provide additional insight into the modeling process.

$$p(\mathbf{x}_k|\mathbf{x}_{k-1}) = p_{w_k}(\mathbf{x}_k - \mathbf{x}_{k-1}), \tag{2a}$$

$$p(\mathbf{y}_k|\mathbf{x}_k) = p_{v_k}(\mathbf{y}_k - W\mathbf{x}_k), \tag{2b}$$

where, p_{w_k} and p_{v_k} represent density functions of the process and measurement noise respectively. Equation (2a) characterizes the evolution of the activation coefficients over time and (2b) is the *likelihood* of observations as specified by the muscle synergies. We present a schematic description of the proposed model in Fig. 1. The latent system state, i.e., the activation coefficients evolve over time and the muscle synergies relate the system output, i.e., the EMG signal to the activation coefficients.

B. The Muscle Synergy Matrix

Muscle synergies serve as basis functions for muscular activations. They are represented as column vectors in the muscle synergy matrix that forms the observation model. For the case of m muscles and n muscle synergies, we have

$$\mathbf{y}_k = W\mathbf{x}_k, \tag{3}$$

where $W = \{w_{ij}\}_{i=1,j=1}^{m,n}$ is the synergy matrix of size $m \times n$, $\mathbf{y}_k = [y_k^1, \ldots, y_k^m]^T$ is the muscle activation vector (EMG

This article has been accepted for publication in a future issue of this journal, but has not been fully edited. Content may change prior to final publication. Citation information: DOI 10.1109/TNSRE.2015.2410176, IEEE Transactions on Neural Systems and Rehabilitation Engineering

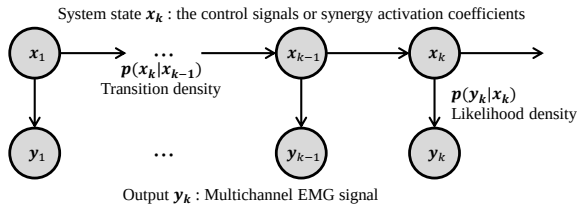

Fig. 1. The proposed mathematical model. The activation coefficients evolve over time and are modeled as the system state. The system output is the EMG signal. The hypothesis of muscle synergies relates the output to the latent system state.

signal) and $\mathbf{x}_k = [x_k^1, \ldots, x_k^n]^T$ are the activation coefficients. To obtain task-specific muscle synergies, we consider K trials of a given task, resulting in consolidated output matrix given as:

$$Y_{m\times K} = W_{m\times n} \times X_{n\times K}, \tag{4}$$

where the subscripts in (4) indicate matrix dimensions. In the above relation, the matrices W and X are unknown while Y is a known quantity. Various unsupervised learning algorithms can be employed to estimate the parameters of the mixing system W and the true physical sources X [24]. Such algorithms exploit *a priori* knowledge about the true nature or structure of the hidden variables such as non-negativity, statistical independence, sparseness, spatio-temporal de-correlation, smoothness, and the lowest possible complexity [24].

In the case of muscle synergies, several separation algorithms have been suggested that include principal component analysis (PCA), factor analysis (FA), independent component analysis (ICA), nonnegative matrix factorization (NMF), and probabilistic ICA (pICA) [11]. Our preliminary investigation into the various algorithms showed that the pICA algorithm performs better than all others for the proposed scheme. We accordingly employ the mean field approach to estimate the synergies W and their corresponding activation coefficients X [25]. Furthermore, we enforce a non-negativity condition on all elements of the mixing matrix and the sources, i.e., $W \succeq 0$ and $X \succeq 0$, where $\succeq$ implies element-wise inequality. Using the pICA algorithm, we estimate q task-specific synergy matrices, i.e., $\{W^i\}_{i=1}^q$, where q is the total number of tasks considered in the experiment, i.e.,

$$[W^i, X^i] = \text{pICA}(Y^i) \quad i = 1, \ldots, q. \tag{5}$$

A representative set of muscle synergies from a participant hand movement are shown in Fig. 2. The synergies were extracted from the EMG data recorded with eight equally-spaced EMG electrodes placed around the forearm while the participant performed six single-DOF tasks. Prior to synergy extraction (by the pICA algorithm), non-overlapping analysis windows (250 ms) were formed from the raw EMG data and root mean square (RMS) values were calculated. The figure represents the contribution of different muscles (or parts of a muscle under the particular EMG channel) for performing various tasks. It is evident from the plots that the synergies are different between tasks. Such a difference in synergies between various tasks relates to the task-specificity of these

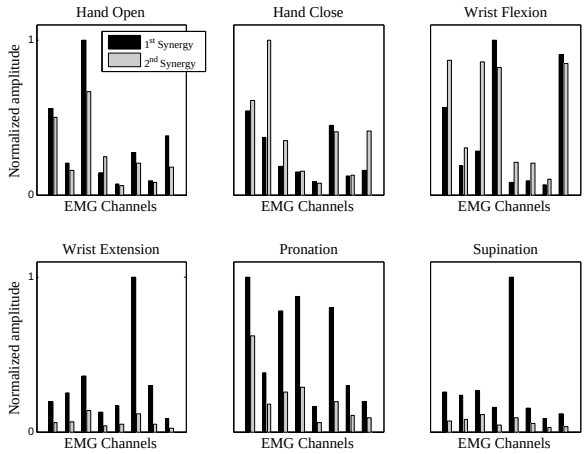

Fig. 2. Representative synergies extracted using the pICA for the first participant. For every single-DOF task, two muscle synergies were extracted from the processed EMG data. The synergy coefficients have been normalized to the maximum value.

muscle synergies. The same phenomenon is later exploited by the proposed MSD algorithm for task discrimination.

C. The Activation Coefficients

The muscle synergy matrices $\{W^i\}_{i=1}^q$ obtained from the pICA algorithm completely specify the proposed state-space model (1) for the given task. Since we have adopted a linear observation model with additive zero-mean white Gaussian noise, the Kalman filter is the optimal recursive Bayesian estimator for such systems [22]. Given the measurement $\mathbf{y}_k$ at time k, the Kalman filter recursively estimates the state $\tilde{\mathbf{x}}_k$. We initialized the Kalman filter with the system state $\mathbf{x}_{0|0} = 0$ and state covariance $P_{0|0} = M$, where M is a randomly generated positive definite matrix with large values. The large values in the covariance matrix indicate a lack of confidence in our initial state, i.e., $\mathbf{x}_{0|0} = 0$ [22]. For the process and measurement noise statistics, we first estimated their covariance matrices (Q_k and R_k respectively) using the Autocovariance Least-Squares (ALS) method [26]. Later, the Kalman filter was manually tuned using the following procedure: the filter was run in the off-line mode and the estimated system state was used to reconstruct muscle activations using synergy matrices [27]. An RMS error was calculated between the actual and the estimated muscle activations. The process and measurement noise statistics were tuned to minimize the RMS error. We used the pilot EMG data from a participant for estimation of noise statistics and tuning the Kalman filter. The estimated statistics were later used for all subsequent testing (real-time as well as off-line) in the study. In Fig. 3, we show the effect of process noise on the state estimation accuracy for a participant during the hand open task. The EMG data was processed to form analysis windows of 250 milliseconds (ms) and the pICA algorithm was used to extract three muscle synergies.

D. The Kalman Filtering

Once a measurement $\mathbf{y}_k$ in the form of EMG data is available, we run q Kalman filters in parallel, one for each

This article has been accepted for publication in a future issue of this journal, but has not been fully edited. Content may change prior to final publication. Citation information: DOI 10.1109/TNSRE.2015.2410176, IEEE Transactions on Neural Systems and Rehabilitation Engineering

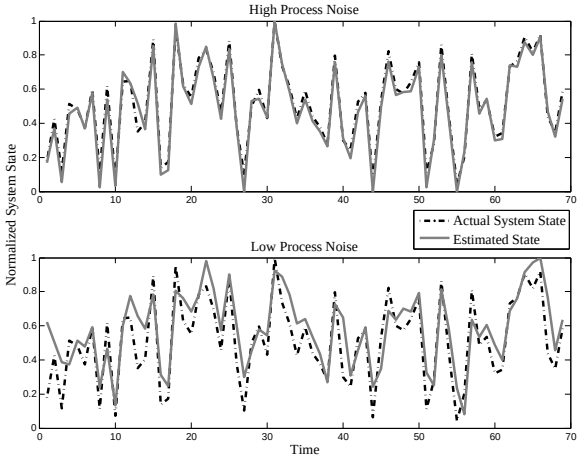

Fig. 3. The effect of process noise on state estimation from EMG data collected during hand-open task. For high process noise, the nature of the process dynamics model (random walk) ensures that the Kalman filter's search-space for the unknown system state is adequately large, thus leading to a better approximation of the unknown state. The time points on the horizontal axis refer to the analysis windows. The state vector consisted of three coefficients, out of which only one is shown here.

synergy matrix $\{W^i\}_{i=1}^q$ in the measurement model. Our formulation of the problem restricts the state estimates to be non-negative, i.e., $\tilde{\mathbf{x}}_k \succeq 0$; however, such a constraint cannot be directly incorporated into the Kalman filter framework. However, we can modify the Kalman filter in a suitable way [28]. Various approaches for modifying the Kalman filter in the presence of constraints have been proposed [28]. We used the projection-based approach, where the estimated state $\tilde{\mathbf{x}}$ is projected onto a nonnegative subspace to find a non-negative state estimate $\hat{\mathbf{x}}$ [29], i.e.

$$\hat{\mathbf{x}} = \underset{\hat{\mathbf{x}}}{\operatorname{argmin}} (\hat{\mathbf{x}} - \tilde{\mathbf{x}})^T \Phi (\hat{\mathbf{x}} - \tilde{\mathbf{x}}), \quad \text{such that} \quad \hat{\mathbf{x}} \succeq 0, \tag{6}$$

where Φ is a positive definite weighting matrix. It can be verified that for $\Phi = I_{n_x}$, the optimization problem in (6) results in a non-negative solution, where all negative elements in the estimated state are replaced with zeros. The estimated states from the q Kalman filters along with their corresponding task-specific synergy matrices are subsequently used for the task discrimination.

E. The Task Discrimination

The proposed scheme for task discrimination is based on the assumption that for a specific task, the pair consisting of the relevant task-specific synergy matrix and its activation coefficients $\{W^z,\ \hat{\mathbf{x}}_k^z\}$ will reconstruct the actual muscle activations $\mathbf{y}_k$ better than all others $\{W^i,\ \hat{\mathbf{x}}_k^i\}_{i=1,i\neq z}^q$. To find this pair, we run q Kalman filters in parallel using all synergy matrices $\{W^i\}_{i=1}^q$ in the measurement model, and find q state estimates $\{\hat{\mathbf{x}}_k^i\}_{i=1}^q$. For each pair, $\{W^i,\ \hat{\mathbf{x}}_k^i\}_{i=1}^q$, we find the estimated muscle activations $\hat{\mathbf{y}}_k^i$ using

$$\hat{\mathbf{y}}_k^i = W^i \hat{\mathbf{x}}_k^i, \quad i = 1, \ldots, q. \tag{7}$$

To assess which pair $\{W^i,\ \hat{\mathbf{x}}_k^i\}$ out of all q pairs best reconstructs the actual state, we employ a similarity measure (SM) that finds a representative real number (called the similarity index) based on the similarity between the estimated $\{\hat{\mathbf{y}}_k^i\}_{i=1}^q$ and actual muscle activations $\mathbf{y}_k$, i.e.,

$$d_k^i = \text{SM}[\hat{\mathbf{y}}_k^i, \mathbf{y}_k], \quad i = 1, \ldots, q. \tag{8}$$

We can employ various similarity measures, e.g., cosine similarity, the sample Pearson correlation coefficient, the Euclidean, or the coefficient of determination r^2. All similarity measures are formally defined in the Appendix and their comparison is presented in Section IV-C. Finally, we find the index of the maximum of all similarity indexes $\{d_k^i\}_{i=1}^q$, i.e.

$$I_k^{MSD} = \text{maxI}[d_k^1, \ldots, d_k^q], \tag{9}$$

where the function maxI finds the index of the maximum of its argument. The resulting index value I_k^{MSD} represents the performed task at time k.

F. The Post-Processing

The post-processing uses the results from LDA to improve the discrimination accuracy of the proposed scheme. The motivation for the post-processing stems from the observation that the MSD and the LDA generally show a low probability of committing the same misclassification. The post-processing routine is invoked when a conflicting decision results from the LDA and the MSD algorithms, i.e., when $I_k^{LDA} \neq I_k^{MSD}$. In such event, we make use of the posterior probability $p_k(I_k|y_k)$ calculated by the LDA and the similarity index d_k calculated by the similarity measure function in Eq. (8). The intuition is that if the LDA posterior probability is high enough ($Th_1 \geq 0.98$) and the LDA decision lies within a ($Th_2 \leq 2.5\%$) neighborhood of the MSD similarity index d_k, then we choose the LDA decision. In all other cases, we choose the MSD decision. For instance, consider the case where the LDA results in the decision "hand open" with posterior probability 99%, and the MSD results in the decision "supination" with a similarity index $d_k = 8$. If the decision "hand open" is within the MSD neighborhood $6 \leq d_k \leq 10$, we decide "hand open". Otherwise, we decide "supination". We tuned the threshold values (Th_1 and Th_2) in the off-line mode using pilot EMG data from a participant. Later, we used the same threshold values for all real-time as well as off-line testing for all participants. The post-processing part of the algorithm significantly increased the task discrimination accuracy ($p < .001$).

G. The Algorithms

The input for the proposed MSD scheme is the multichannel EMG data and its output is the identified task. The MSD scheme consists of two stages.

1) Offline task-specific synergies extraction. The recorded EMG data from the training session is processed and divided into multiple bins, where each bin corresponds to a specific task (Algorithm-I). By employing the pICA, we obtain task-specific muscle synergies from each bin using Eq. (5). Additionally, the LDA coefficients are calculated to be used later in the post-processing.
2) Real-time task discrimination. The EMG data is buffered for a certain duration as specified by the analysis window

This article has been accepted for publication in a future issue of this journal, but has not been fully edited. Content may change prior to final publication. Citation information: DOI 10.1109/TNSRE.2015.2410176, IEEE Transactions on Neural Systems and Rehabilitation Engineering

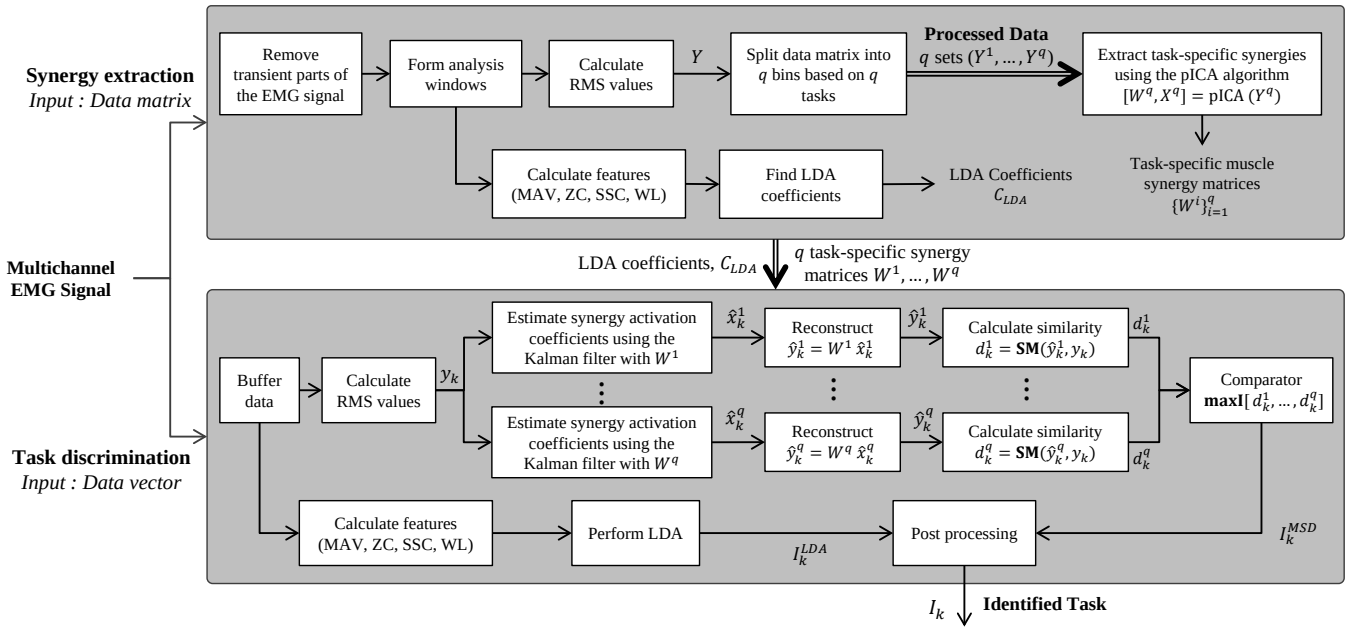

Fig. 4. A schematic layout of the proposed MSD algorithm for task discrimination using task-specific muscle synergies. The input to the MSD algorithm is a multichannel EMG signal and the output is the identified task I_k. The algorithm consists of two sequential stages. In the first stage, task-specific muscle synergies are extracted using the pICA algorithm, while in the second stage task discrimination is performed in real-time. Abbreviations used are, MAV : Mean Absolute Value, ZC : Zero Crossing, SSC : Slope Sign Change, WL : Waveform Length. Definitions and further details about LDA features can be found in [1].

Algorithm-I : Task-specific synergy extraction.

Inputs: Raw EMG data Y, Number of tasks q.
Outputs: Task-specific synergy matrices $\{W^i\}_{i=1}^q$, LDA coefficients C_{LDA}.
Parameters: Contraction time percentage (cTp), Analysis window size T_a, Window increment time T_{inc}.

procedure $[W^i, C_{LDA}]$ = EXTRACT SYNERGY(Y, q)
  Remove transient parts of the EMG data.
  Form analysis windows and calculate RMS values.
  Segment RMS data into q bins $\{Y^i\}_{i=1}^q$.
  for $i = 1 : q$ **do**
    $[W^i, X^i] = \text{pICA}(Y^i)$
  end for
  C_{LDA} = LDA (Y)
end procedure

Algorithm-II : Task discrimination.

Inputs: Raw EMG data y, $\{W^i\}_{i=1}^q$, C_{LDA}.
Outputs: I_k.
Parameters: cTp, T_a, T_{inc}.

procedure $[I_k]$ = DISCRIMINATE$(y, \{W^i\}_{i=1}^q, C_{LDA})$
  Buffer and calculate RMS values of the EMG data.
  Initialize Kalman filter (KF), $x_{0|0}$, $P_{0|0}$, Q_0, and R_0.
  for $i = 1 : q$ **do**
    $\hat{x}_k^i$ = KF (y_k)
    $\hat{y}_k^i = W^i \hat{x}_k^i$
    d_k^i = SM $(y_k, \hat{y}_k^i)$
  end for
  I_k^{MSD}= maxI $[d_k^1, \ldots, d_k^q]$
  $[I_k^{LDA}, p_k(I|y_k)]$ = LDA (y_k, C_{LDA})
  if $I_k^{LDA} \neq I_k^{MSD}$ **then**
    I_k = PostProc $(I_k^{MSD}, d_k^i, I_k^{LDA}, p_k(I|y_k))$
  end if
end procedure

size (see Section IV-B), processed and passed on to the Kalman filters for estimation of the activation coefficients followed by task discrimination (Algorithm-II). In the case of a conflicting decision by the MSD and the LDA, post-processing (Algorithm-III) is performed to reduce the possibility of error.

A schematic representation of the MSD algorithm is presented in Fig. 4, while detailed description for the synergy extraction, task discrimination and post-processing are presented in Algorithm-I, -II and -III.

III. EXPERIMENTAL METHODS

The study received approval from the Institutional Review Board of the University of Arkansas at Little Rock. A total of twelve volunteers (height 171.4±8.8 cm (mean±std), mass 73.2±12.3 Kg and age 28.2±6.5 years) participated in the study. A written informed consent was obtained from all participants before start of the data collection. All participants were right hand dominant with no known history of neuromuscular disorders.

This article has been accepted for publication in a future issue of this journal, but has not been fully edited. Content may change prior to final publication. Citation information: DOI 10.1109/TNSRE.2015.2410176, IEEE Transactions on Neural Systems and Rehabilitation Engineering

Algorithm-III : Post processing.

Inputs: $I_k^{MSD}, d_k^i, I_k^{LDA}, p_k(I|y_k)$.
Outputs: I_k.
Parameters: $Th_1 = 98\%$, $Th_2 = 2.5\%$ of d_k^I.

procedure I_k = POSTPROC($I_k^{MSD}, d_k^i, I_k^{LDA}, p_k(I|y_k)$)
  $I_k = I_k^{MSD}$
  if $p_k(I_k^{LDA}|y_k) \geq Th_1$ **then**
    if I_k^{LDA} within Th_2 **then**
      $I_k = I_k^{LDA}$
    end if
  else if $I_{k-1} = I_{k-2}$ **then**
    $I_k = I_{k-1}$
  end if
end procedure

A. Experimental Design

1) Tasks: For each participant, we record data in two separate sessions on the same day. The first session consisted of single-DOF tasks (six in total), and the second session consisted of single as well as multi-DOF tasks (18 in total). The first session (referred to as 1-DOF tasks) consisted of hand open/close, wrist flexion/extension, and forearm pronation/supination. The second session included six 1-DOF tasks and twelve multi-DOF tasks, i.e., all possible pairs of 1-DOF tasks, open + flex hand, close + flex hand, open + extend hand, close + extend hand, open hand + pronation, close hand + pronation, open hand + supination, close hand + supination, flex hand + pronation, extend hand + pronation, flex hand + supination, and extend hand + supination (referred to 1+2-DOF tasks).

2) Electrode Configuration: In order to record EMG data from the forearm, we considered two possible electrode configurations, i.e., muscle targeting and symmetrical arrangement. For muscle targeting, we used the configuration proposed by Farrell and Weir [30]. For a symmetrical arrangement, we placed five electrodes around the circumference of the forearm symmetrically with the first electrode placed beneath in line with the medial epicondyle of the humerus. Electrodes were placed around the proximal end of the forearm at a location $1/3$ of the distance between medial epicondyle of the humerus and styloid process of the ulna.

B. EMG Data Recording

We used Noraxon TeleMyo Direct Transmission System (DTS) (Noraxon USA Inc) with wireless sensors to record the EMG data. This equipment has inbuilt filtering scheme (band-pass filter of 10-500 Hz) and provides a single differential data. We used disposable, self-adhesive silver/silver chloride (Ag/AgCl) snap electrodes with two circular conductive areas of 1 cm each and an inter-electrode distance of 2 cm. We used a NI-USB 6009 (National Instruments Corporation, Austin, Texas) data acquisition card to acquire and digitize the EMG data at the rate of 2000 samples per second. We modified the BioPatRec software to acquire and process the EMG data [31]. A schematic layout of the experimental setup is given in Fig. 5. Before start of the data collection, each participant sat comfortably in a chair with right arm resting over a table in front. Visual cues were provided to participants to guide them throughout the data collection process. Participants performed each task for 5 secs with a 5 sec rest between two consecutive tasks. A single trial consisted of performing all tasks once. Participants were instructed to maintain a comfortable and repeatable force level for all tasks.

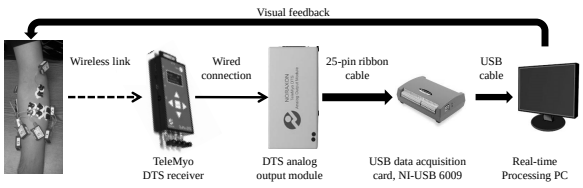

Fig. 5. The hardware setup for EMG data collection.

C. Data Analysis

In order to expound the efficacy of the proposed scheme, we performed detailed investigation in two distinct modes, i.e., off-line mode and real-time mode. In the off-line analysis both data sets (1-DOF tasks and 1+2-DOF tasks) were processed under various conditions and parameter values. The real-time testing was performed only on the 1-DOF tasks using the TAC test.

We evaluated the performance of the MSD algorithm for various parameters and under different conditions, i.e., the analysis window size T_a, window time increment T_{inc}, number of task-specific muscle synergies, contraction time percentage (cTp), processing time T_p, training time, EMG electrode arrangement and similarity measures. For the purpose of performance evaluation, the EMG data from all trials was randomly divided into two bins with 75% of the data in the first bin and the remaining 25% in the second bin. The first bin was used for synergy extraction (or training for other classification algorithms) while the second bin was used for task discrimination (i.e., cross-validation). Task discrimination accuracies reported are average values across all runs (fifteen in total) for all participants.

We employed the TAC test to evaluate the MSD algorithm in a real-time environment. Participants 3 and 9 could not complete the TAC test and therefore were excluded from the results. Both participants felt that the control of the virtual prosthetic hand was unintuitive and reported fatigue after making various efforts using both algorithms, i.e., the LDA and the MSD. All the remaining participants performed six 1-DOF tasks with both the MSD and the LDA in a single session. We assumed that training and familiarization with the experiment may have a significant impact on the TAC test. Therefore, we randomized the order in which participants performed TAC test with the MSD or the LDA, i.e., five participants performed the TAC test first with the LDA and other five performed it with the MSD first. Both algorithms were analyzed using three metrics, i.e., task completion rate, task completion time, and the path efficiency [17]. Both algorithms were tested

This article has been accepted for publication in a future issue of this journal, but has not been fully edited. Content may change prior to final publication. Citation information: DOI 10.1109/TNSRE.2015.2410176, IEEE Transactions on Neural Systems and Rehabilitation Engineering

using the following parameter selections: number of trials = 2, repetitions = 3, test time = 15 secs, allowed range = 5 degrees, and dwell time = 1 sec.

Identifying the number of synergies yielding the best discrimination accuracy is important for the MSD algorithm. The variance accounted for (VAF) is a common metric used to ascertain the correct number of synergies required to represent the data effectively in a low dimensional subspace. An increase in the number of muscle synergies usually results in an increased VAF. However, the effect of VAF on the task discrimination accuracy was not evident. Therefore, we considered the task discrimination accuracy to quantify the effect of the number of synergies on the MSD algorithm.

It is known that the decision stream, i.e., the number of discrimination decisions per unit time provided by the algorithm, should be as dense as possible [32]. The density of the decision stream is directly affected by T_p and T_{inc}. Keeping the processing times $T_p = 3$ secs in mind, we chose a value of 10 ms for T_{inc}, i.e., a discrimination decision will be available after every 10 ms in real-time.

Transient parts of the EMG signal at the initiation and termination of a movement affect the task discrimination accuracy of the algorithm. We can specify the cTp in the MSD algorithm and control how much of the transient information is available for synergy extraction (i.e., off-line processing). A cTp value of 50% will remove all transient information (from both sides of the signal) while a value of 100% will retain all information. With an increase in the cTp value, as expected, the discrimination accuracy decreases. However, it is known that including the transient information of the EMG signal into discrimination algorithms improves the real-time performance, albeit a decrease in the off-line accuracy [33]. In this respect, a cTp of 70% provides an acceptable compromise between off-line accuracy and real-time performance [31].

We compared discrimination errors of the MSD algorithm with three other algorithms: 1) the LDA, 2) the artificial neural network (ANN), 3) one-vs-all support vector machine (SVM). We used a common set of EMG features (MAV, ZC, SSC, and WL [1], [3]) for all three algorithms. All four algorithms were tested under identical conditions using the same EMG data (e.g., the amount of training and testing EMG data, the number of movement classes, and number of EMG channels and features). We used an analysis window $T_a = 250$ ms, window increment time $T_{inc} = 150$ ms and cTp = 0.7 for the EMG data. We selected a feed-forward ANN with one hidden layer having five neurons. The output layer had neurons equal to the number of tasks (that included all movements plus a 'rest' class, i.e., 7 for 1-DOF and 19 for 1+2-DOF). The ANN was trained using the Levenberg-Marquardt backpropagation algorithm.

All statistical tests, i.e., repeated measure analysis of variance (ANOVA) with a Greenhouse-Geisser correction and post hoc investigations using the Bonferroni correction (where required) were performed using IBM SPSS version 22. All statistical tests were performed at a 95% significance level.

IV. Results

A. Number of Task-Specific Muscle Synergies

In Fig. 6(a) we present the task discrimination accuracy as a function of the number of muscle synergies (1 through 6) for both data sets. We found significant synergies effects on the discrimination accuracy ($p < .001$) for both data sets. Investigation using pairwise comparisons showed that two or more synergies were sufficient to achieve maximum task discrimination accuracy for 1-DOF tasks ($p < .01$). Any further increase in the number of synergies did not significantly improve discrimination accuracy. An investigation along the same lines for 1+2-DOF tasks found that three synergies were sufficient for maximum discrimination accuracy.

B. Analysis Window Size (T_a)

The analysis window size, T_a controls the amount of information available to the MSD algorithm for task discrimination and therefore directly affects its performance. We analyzed the MSD algorithm for different analysis window sizes, starting from 100 ms to 400 ms with an increment of 50 ms as shown in Fig. 6(b). Repeated measure ANOVA showed a significant effect for the window size ($p < .001$) on the task discrimination accuracy for both data sets. A post hoc investigation revealed that an increase in T_a provided a significant increase in the task discrimination accuracy. However, due to the real-time requirements, T_a cannot be increased arbitrarily. In [34], the following relationship between T_a, increment time T_{inc}, processing time T_p, and the controller delay D was suggested:

$$D = \frac{1}{2}T_a + \frac{1}{2}T_{inc} + T_p, \tag{10}$$

We selected $T_a = 250$ ms, $T_{inc} = 10$ ms, and $T_p = 3$ ms (see Fig. 6(c) for T_p), which corresponded to a controller delay of $D = 133$ ms. The resulting value is slightly higher than the acceptable value of 120 ms [35], however, the selected parameters, i.e., $T_a = 250$ ms and $T_{inc} = 10$ ms provided good performance in real-time.

C. Similarity Measures

Similarity measures were employed to ascertain how close the estimated muscle activations $\hat{y}_k^i$ are to the actual ones y_k. We investigated four different similarity measures in this study, including a cosine similarity measure, the Euclidean distance, the Pearson correlation coefficient, and the coefficient of determination r^2 (defined in Appendix). The differences between all four similarity measures were not considered statistically significant ($p = .149$).

D. Real-time processing and Synergy Extraction Times

The real-time processing corresponds to the time required by the MSD algorithm to execute a single measurement of the EMG signal, while the synergy extraction time can be considered as the training time for the proposed MSD algorithm. In Fig. 6(c), we show the time consumed by the MSD algorithm to process a single measurement for task discrimination using various numbers of synergies. We also present the time consumed by the algorithm to extract the synergy matrices (right vertical axis in Fig. 6(c)).

This article has been accepted for publication in a future issue of this journal, but has not been fully edited. Content may change prior to final publication. Citation information: DOI 10.1109/TNSRE.2015.2410176, IEEE Transactions on Neural Systems and Rehabilitation Engineering

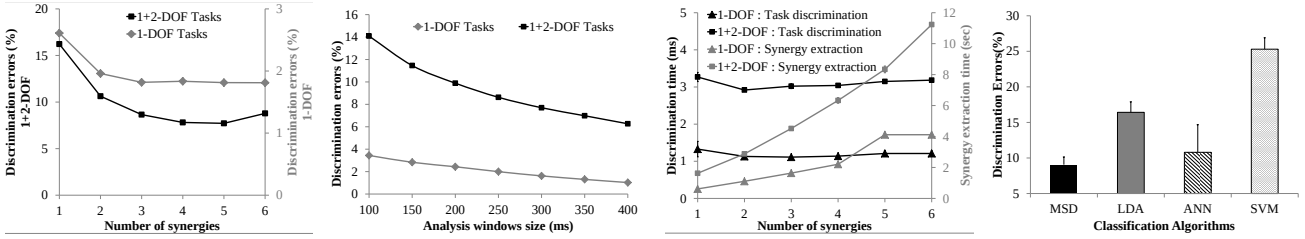

(a) Muscle synergies (b) Analysis windows size T_a (c) Processing time (d) Comparison with the other classification algorithms

Fig. 6. Performance analyses of the MSD algorithm. (a) Effect of the number of synergies on the task discrimination errors for 1-DOF and 1+2-DOF tasks. (b) Effect of the analysis window size T_a on the task discrimination errors (a value of T_{inc}=10 ms was used for all window sizes). (c) Time required for extraction of muscle synergies and task discrimination. (d) Comparison of the proposed MSD algorithm with other classification algorithms in terms of discrimination errors (The boxes' heights correspond to the mean discrimination error and the vertical bar above each box corresponds to one standard deviation of the error).

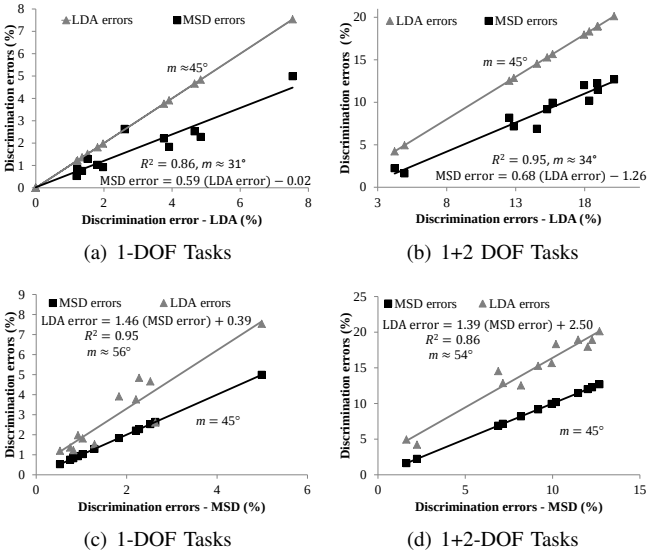

(a) 1-DOF Tasks (b) 1+2 DOF Tasks

(c) 1-DOF Tasks (d) 1+2-DOF Tasks

Fig. 7. Robustness analysis of the proposed MSD algorithm. The discrimination errors of both the LDA and the MSD algorithm are plotted against the LDA errors (top row) and against the MSD errors (bottom row) for all twelve participants for individual data sets (1-DOF tasks and 1+2-DOF tasks).

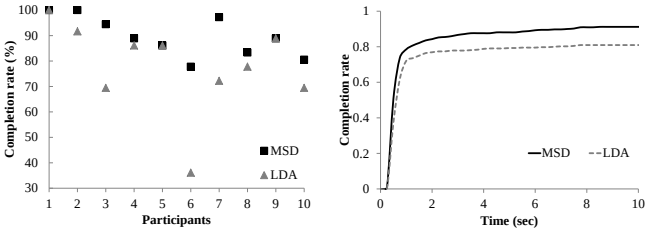

(a) Individual completion rate (b) Cumulative completion rate

Fig. 8. Completion rates for the TAC test. (a) Individual completion rate are shown where each marker represents a participant's completion rate using the LDA (blue triangular marker) or the MSD algorithm (black square marker). (b) Cumulative completion rate for all participants showing average performance of both algorithms.

E. Comparison with the Other Classification Algorithms

Figure 6(d) shows the mean and standard deviation of the discrimination error for the different algorithms (MSD, LDA, ANN and SVM). The boxes' heights correspond to the mean discrimination error and the vertical bar above each box corresponds to one standard deviation of the error. We found statistically significant differences between discrimination accuracies $p < .001$. Further investigation using pairwise comparison showed that differences between means of all groups were significant $p < .001$, except for the MSD and ANN $p = .147$. At the same time, a large variance in the ANN classification accuracy as compared to the MSD was observed, which was later verified with the Levene's test of equality of variances $(p < .001)$.

F. Robustness of the MSD Algorithm

We hypothesized that the proposed MSD algorithm is more robust to discrimination errors than the widely used LDA. To test our hypothesis, we analyzed the discrimination errors of both algorithms for all twelve participants (Fig. 7). In Figs. 7(a) and 7(b), we present discrimination errors of the MSD and the LDA plotted against the LDA error for 1-DOF and 1+2-DOF data sets, respectively. In both Figs., each marker represents a particular participant. The blue triangular markers show the average LDA discrimination error, while the black square markers indicate the average MSD discrimination error. The blue lines, with a slope $m = 45°$ in both Figs., show the LDA errors plotted against the LDA errors. Once we performed a linear fit to MSD errors (black lines), we found that the fitted lines had lower slope values, i.e., $m = 31°$ for 1-DOF tasks and $m = 34°$ for 1+2-DOF tasks. These slope values indicate that the rate of increase of the MSD error is lower than that of LDA, i.e., once the LDA error grows, the MSD error grows at a lower rate, i.e., when the LDA has an error rate of 1, the MSD algorithm has error rates of 0.59 and 0.68 for 1-DOF and 1+2-DOF tasks, respectively. These results show that the proposed MSD algorithm is relatively more robust to discrimination errors. Similar and supporting results were found by plotting discrimination errors of both algorithms against the MSD error (Fig. 7(c) and Fig. 7(d)), where the LDA exhibits a higher discrimination error increase rate.

G. Real-time Testing using the TAC Test

Results of the TAC test for both algorithms are given in Table I. The values presented in the table are averaged across all tasks for all participants. The superior performance of the

This article has been accepted for publication in a future issue of this journal, but has not been fully edited. Content may change prior to final publication. Citation information: DOI 10.1109/TNSRE.2015.2410176, IEEE Transactions on Neural Systems and Rehabilitation Engineering

TABLE I
TAC TEST RESULTS

Metric	MSD (mean+std)	LDA (mean+std)
Completion rate	0.90±0.19	0.78±0.27
Completion time (secs)	4.92 ±1.11	4.95 ±1.13
Path efficiency	0.95±0.06	0.93±0.08

MSD algorithm is evident from the task completion rate ($p < .01$) as shown in Fig. 8. There were no significant difference observed in completion time and path efficiency. However, these two parameters are calculated for completed tasks only and therefore should be interpreted in the light of the task completion rate.

V. DISCUSSION

We formulated the problem of task discrimination as a real-time estimation problem of activation coefficients within a state-space dynamical model. The proposed MSD algorithm for real-time task discrimination is both efficient and robust. The real-time part of the MSD algorithm, which consists of estimating the activation coefficients, task discrimination and post-processing, is executed in approximately 1 ms (Lenovo IdeaPad Y500 Laptop) for 1-DOF tasks and 3 ms for 1+2-DOF tasks. For the training time, in the current setting the participants perform each task for 5 secs with a 5 sec rest between two tasks and each task was repeated three times. In this scenario, the total training time for 1-DOF tasks is about 2 mins and 45 sec (inclusive of all breaks). The holding time for each task and inter-task break can be reduced from 5 secs to 3 secs without compromising the average discrimination accuracy [36]. In this case, the training time is reduced to approximately 99 secs for 1-DOF tasks and 5 mins and 15 secs for 1+2-DOF (18 tasks).

Our investigation revealed no differences between muscle targeting or symmetrical arrangement of electrodes for EMG data collection, which confirmed earlier results [30], prompting us to proceed with a symmetrical arrangement of electrodes.

The number of task-specific muscle synergies directly influences the performance of the MSD algorithm. We found that, in general, three or more synergies provide a superior discrimination accuracy for all possible tasks (1-DOF as well as 1+2-DOF tasks). Therefore, we recommend using three muscle synergies for the general discrimination problem. Our investigation into the analysis window size T_a led us to select a value of 250 ms, which is supported by previous research [32]. Furthermore, due to the fact that we have $T_p = 3$ ms for 1+2 DOF tasks, we may choose a $T_{inc} > 10$ ms to provide a dense decision stream.

Various machine learning algorithms including the LDA, quadratic discriminant analysis, different flavors of ANN, k-nearest neighbors, and SVMs have been tried in myoelectric control. Nevertheless, all classifiers perform equally well and no statistical differences have been reported in their classification accuracies [37]. We compared the performance of the MSD algorithm with three of them: the LDA, feed-forward ANN and the one-vs-all SVM, and found that the MSD algorithm performs better than others in terms of off-line classification accuracy ($p < .05$) except for the ANN. However, an increased training time along with a higher value of variance ($p < .001$) was observed for the ANN.

We showed that the proposed MSD algorithm is robust to misclassification in the presence of a degrading EMG signal. As the error rate of the LDA increases, the MSD discrimination errors increase at a significantly lower rate. An ideal discrimination scheme will have a horizontal line (a line with slope zero) in Fig. 7, meaning in the presence of classification errors by an algorithm, the ideal scheme performs robustly with no effect on the discrimination accuracy. In this respect, the MSD algorithm ($m = 31^\circ$ and $m = 34^\circ$ for 1-DOF and 1+2-DOF tasks, respectively) is relatively more robust than the LDA ($m = 45^\circ$). Therefore, we infer that for users (e.g., amputees) with lower amplitude/noisy EMG signals, the MSD algorithm will perform more robustly and provide comparatively higher discrimination accuracies.

We considered a linear form process dynamics and observation model, which may be a simplification of the underlying physical phenomenon. We acknowledge that a nonlinear model would likely improve the performance of the proposed MSD algorithm in terms of classification accuracy as well as real-time controllability. However, with a nonlinear system model, the Kalman filter cannot be used for the estimation of the activation coefficients and will need to be replaced by a nonlinear Bayesian estimator, such as the extended Kalman filter, unscented Kalman filter, or the Particle filter. The non-negativity constraint on the latent system state further complicates the estimation of activation coefficients. Additionally, the computational demands of nonlinear estimation techniques may prohibit their use for real-time application.

We used a modified form of the Kalman filter for the synergy coefficient estimation due to the non-negativity constraint on the unknown system state. Though different methodologies can be adopted to constrain the unknown state, for a linear system with linear constraints all methods result in similar state estimate [28].

We have shown, using the TAC test, that the proposed MSD algorithm performs better than the LDA especially in terms of *task completion rate*, with $p < .01$. From Table I, we see that for other two metrics, i.e., *completion time* and *path efficiency*, the MSD algorithm again performs better than the LDA, though differences may not be significant. However, it is important to highlight that these two metrics are calculated only from the completed tasks (i.e., excluding data of all tasks which were not completed).

VI. CONCLUSION

We have presented a new conceptual and computational scheme to address the challenging problem of real-time task discrimination for myoelectric control. The problem was formulated in a new way using state-space representation and the task-specific muscle synergies. The proposed discrimination algorithm is robust and outperforms other commonly employed classification algorithms both in terms of off-line accuracy as well as real-time performance ($p < .01$).

This article has been accepted for publication in a future issue of this journal, but has not been fully edited. Content may change prior to final publication. Citation information: DOI 10.1109/TNSRE.2015.2410176, IEEE Transactions on Neural Systems and Rehabilitation Engineering

APPENDIX
SIMILARITY MEASURES

We used four similarity measures for the MSD algorithm, i.e., cosine similarity, the sample Pearson correlation coefficient, the Euclidean distance, and the coefficient of determination r^2. Given two vectors x_s and x_t, the four measures are defined as:

- Cosine $= x_s^T x_t / \sqrt{x_s^T x_s x_t^T x_t}$, where ^{T} represents transpose.
- Correlation $= \left[x_{ss}^T x_{tt} / \sqrt{x_{ss}^T x_{ss} x_{tt}^T x_{tt}}\right]$, where $x_{ii} = (x_i - \bar{x}_i)$, $\bar{x}_i = \sum_j x_{ij}$.
- Euclidean $= \sqrt{(x_s - x_t)^T (x_s - x_t)}$
- r^2 Index $= \left[(x_s - x_t)^T (x_s - x_t) / (x_s - \bar{x}_s)^T (x_s - \bar{x}_s)\right]$

REFERENCES

[1] S. Micera, J. Carpaneto, and S. Raspopovic, "Control of hand prostheses using peripheral information," *IEEE Reviews in Biomedical Engineering*, vol. 3, pp. 48–68, 2010.

[2] G. Rasool, N. Bouaynaya, K. Iqbal, and G. White, "Surface myoelectric signal classification using the AR-GARCH model," *Biomedical Signal Processing and Control*, vol. 13, pp. 327–336, Sep. 2014.

[3] E. Scheme and K. Englehart, "Electromyogram pattern recognition for control of powered upper-limb prostheses: State of the art and challenges for clinical use," *The Journal of Rehabilitation Research and Development*, vol. 48, no. 6, p. 643, 2011.

[4] B. Peerdeman, D. Boere, H. Witteveen, R. H. in 't Veld, H. Hermens, S. Stramigioli, H. Rietman, P. Veltink, and S. Misra, "Myoelectric forearm prostheses: state of the art from a user-centered perspective," *Journal of Rehabilitation Research and Development*, vol. 48, no. 6, pp. 719–737, 2011.

[5] B. Lock, K. Englehart, and B. Hudgins, "Real-time myoelectric control in a virtual environment to relate usability vs. accuracy," in *Proceedings of the 2005 MyoElectric Controls/Powered Prosthetics Symposium*. Fredericton, New Brunswick, Canada, August 17-19, 2005.

[6] N. Jiang, S. Dosen, K.-R. Muller, and D. Farina, "Myoelectric control of artificial limbs - is there a need to change focus?" *IEEE Signal Processing Magazine*, vol. 29, no. 5, pp. 152–150, Sep. 2012.

[7] E. Scheme, B. Hudgins, and K. Englehart, "Confidence-based rejection for improved pattern recognition myoelectric control," *IEEE Transactions on Biomedical Engineering*, vol. 60, no. 6, pp. 1563–1570, June 2013.

[8] E. Bizzi, V. Cheung, A. d'Avella, P. Saltiel, and M. Tresch, "Combining modules for movement," *Brain Research Reviews*, vol. 57, no. 1, pp. 125–133, Jan. 2008.

[9] A. d'Avella and E. Bizzi, "Shared and specific muscle synergies in natural motor behaviors," *Proceedings of the National Academy of Sciences of the United States of America*, vol. 102, no. 8, pp. 3076–3081, Feb. 2005.

[10] M. Chhabra and R. A. Jacobs, "Properties of synergies arising from a theory of optimal motor behavior," *Neural Computation*, vol. 18, no. 10, pp. 2320–2342, Aug. 2006.

[11] M. C. Tresch, V. C. K. Cheung, and A. d'Avella, "Matrix factorization algorithms for the identification of muscle synergies: evaluation on simulated and experimental data sets," *Journal of Neurophysiology*, vol. 95, no. 4, pp. 2199–2212, Apr. 2006.

[12] M. C. Tresch and A. Jarc, "The case for and against muscle synergies," *Current Opinion in Neurobiology*, vol. 19, no. 6, pp. 601–607, Dec. 2009.

[13] A. Ajoudani, S. B. Godfrey, M. Bianchi, M. G. Catalano, G. Grioli, N. Tsagarakis, and A. Bicchi, "Exploring teleimpedance and tactile feedback for intuitive control of the pisa/IIT SoftHand," *IEEE Transactions on Haptics*, vol. 7, no. 2, pp. 203–215, 2014.

[14] C. Choi and J. Kim, "Synergy matrices to estimate fluid wrist movements by surface electromyography," *Medical Engineering & Physics*, vol. 33, no. 8, pp. 916–923, 2011.

[15] G. C. Matrone, C. Cipriani, M. C. Carrozza, and G. Magenes, "Real-time myoelectric control of a multi-fingered hand prosthesis using principal components analysis," *Journal of NeuroEngineering and Rehabilitation*, vol. 9, no. 40, 2012.

[16] N. Jiang, H. Rehbaum, I. Vujaklija, B. Graimann, and D. Farina, "Intuitive, online, simultaneous, and proportional myoelectric control over two degrees-of-freedom in upper limb amputees," *IEEE Transactions on Neural Systems and Rehabilitation Engineering*, vol. 22, no. 3, pp. 501–510, 2014.

[17] A. Simon, L. Hargrove, B. Lock, and T. Kuiken, "Target achievement control test: Evaluating real-time myoelectric pattern-recognition control of multifunctional upper-limb prostheses," *J Rehabil Res Dev*, vol. 48, no. 6, pp. 619–628, 2011.

[18] A. H. Jazwinski, *Stochastic Processes and Filtering Theory*. Academic Press, Jan. 1970.

[19] M. H. Hayes, *Statistical Digital Signal Processing and Modeling*, 1st ed. New York: Wiley, Apr. 1996.

[20] E. A. Clancy and N. Hogan, "Probability density of the surface electromyogram and its relation to amplitude detectors," *IEEE Transactions on Biomedical Engineering*, vol. 46, no. 6, pp. 730–739, 1999.

[21] K. Nazarpour, A. H. Al-Timemy, G. Bugmann, and A. Jackson, "A note on the probability distribution function of the surface electromyogram signal," *Brain Research Bulletin*, vol. 90, pp. 88–91, Jan. 2013.

[22] D. Simon, *Optimal State Estimation: Kalman, H Infinity, and Nonlinear Approaches*. Wiley-Interscience, Jun. 2006.

[23] S. Thrun, W. Burgard, and D. Fox, *Probabilistic Robotics*. The MIT Press, Aug. 2005.

[24] A. Cichocki, R. Zdunek, A. H. Phan, and S. Amari, *Nonnegative Matrix and Tensor Factorizations: Applications to Exploratory Multi-way Data Analysis and Blind Source Separation*. John Wiley & Sons, Jul. 2009.

[25] P. A. d. F. R. Højen-Sørensen, O. Winther, and L. K. Hansen, "Mean-field approaches to independent component analysis," *Neural Computation*, vol. 14, no. 4, pp. 889–918, 2002.

[26] M. R. Rajamani and J. B. Rawlings, "Estimation of the disturbance structure from data using semidefinite programming and optimal weighting," *Automatica*, vol. 45, no. 1, pp. 142–148, Jan. 2009.

[27] G. Rasool, K. Iqbal, N. Bouaynaya, and G. White, "Neural drive estimation using the hypothesis of muscle synergies and the state-constrained kalman filter," in *6th International IEEE/EMBS Conference on Neural Engineering (NER)*, San Diego, CA, Nov. 2013, pp. 802–805.

[28] D. Simon, "Kalman filtering with state constraints: a survey of linear and nonlinear algorithms," *IET Control Theory Applications*, vol. 4, no. 8, pp. 1303–1318, Aug. 2010.

[29] G. Rasool and N. Bouaynaya, "Inference of time-varying gene networks using constrained and smoothed kalman filtering," in *2012 IEEE International Workshop on Genomic Signal Processing and Statistics, (GENSIPS)*, Washington, DC, Dec. 2012, pp. 172–175.

[30] T. Farrell and R. F. Weir, "A comparison of the effects of electrode implantation and targeting on pattern classification accuracy for prosthesis control," *IEEE Transactions on Biomedical Engineering*, vol. 55, no. 9, pp. 2198–2211, Sep. 2008.

[31] M. Ortiz-Catalan, R. Brånemark, and B. Håkansson, "BioPatRec: a modular research platform for the control of artificial limbs based on pattern recognition algorithms," *Source Code for Biology and Medicine*, vol. 8, no. 11, Apr. 2013.

[32] L. H. Smith, L. J. Hargrove, B. A. Lock, and T. A. Kuiken, "Determining the optimal window length for pattern recognition-based myoelectric control: balancing the competing effects of classification error and controller delay," *IEEE Transactions on Neural Systems and Rehabilitation Engineering*, vol. 19, no. 2, pp. 186–192, Apr. 2011.

[33] L. Hargrove, Y. Losier, B. Lock, K. Englehart, and B. Hudgins, "A real-time pattern recognition based myoelectric control usability study implemented in a virtual environment," in *29th Annual International Conference of the IEEE Engineering in Medicine and Biology Society EMBS*, Aug. 2007, pp. 4842–4845.

[34] T. Farrell and R. F. Weir, "Analysis window induced controller delay for multifunctional prostheses," in *Proceedings of the MEC Symposium Conference Proceedings, UNB*, 2008.

[35] ——, "The optimal controller delay for myoelectric prostheses," *IEEE Transactions on Neural Systems and Rehabilitation Engineering*, vol. 15, no. 1, pp. 111–118, Mar. 2007.

[36] M. Ortiz-Catalan, B. Håkansson, and R. Brånemark, "Real-time and simultaneous control of artificial limbs based on pattern recognition algorithms," *IEEE Transactions on Neural Systems and Rehabilitation Engineering*, vol. 22, no. 4, pp. 756–764, 2014.

[37] L. Hargrove, K. Englehart, and B. Hudgins, "A comparison of surface and intramuscular myoelectric signal classification," *IEEE Transactions on Biomedical Engineering*, vol. 54, no. 5, pp. 847–853, May 2007.